Government of **Western Australia**
Department of **Mines and Petroleum**

RECORD 2016/16

MAPPING IRON ORE ALTERATION PATTERNS IN BANDED IRON-FORMATION USING HYPERSPECTRAL DATA: BEEBYN DEPOSIT, YILGARN CRATON, WESTERN AUSTRALIA

by
P Duuring and C Laukamp

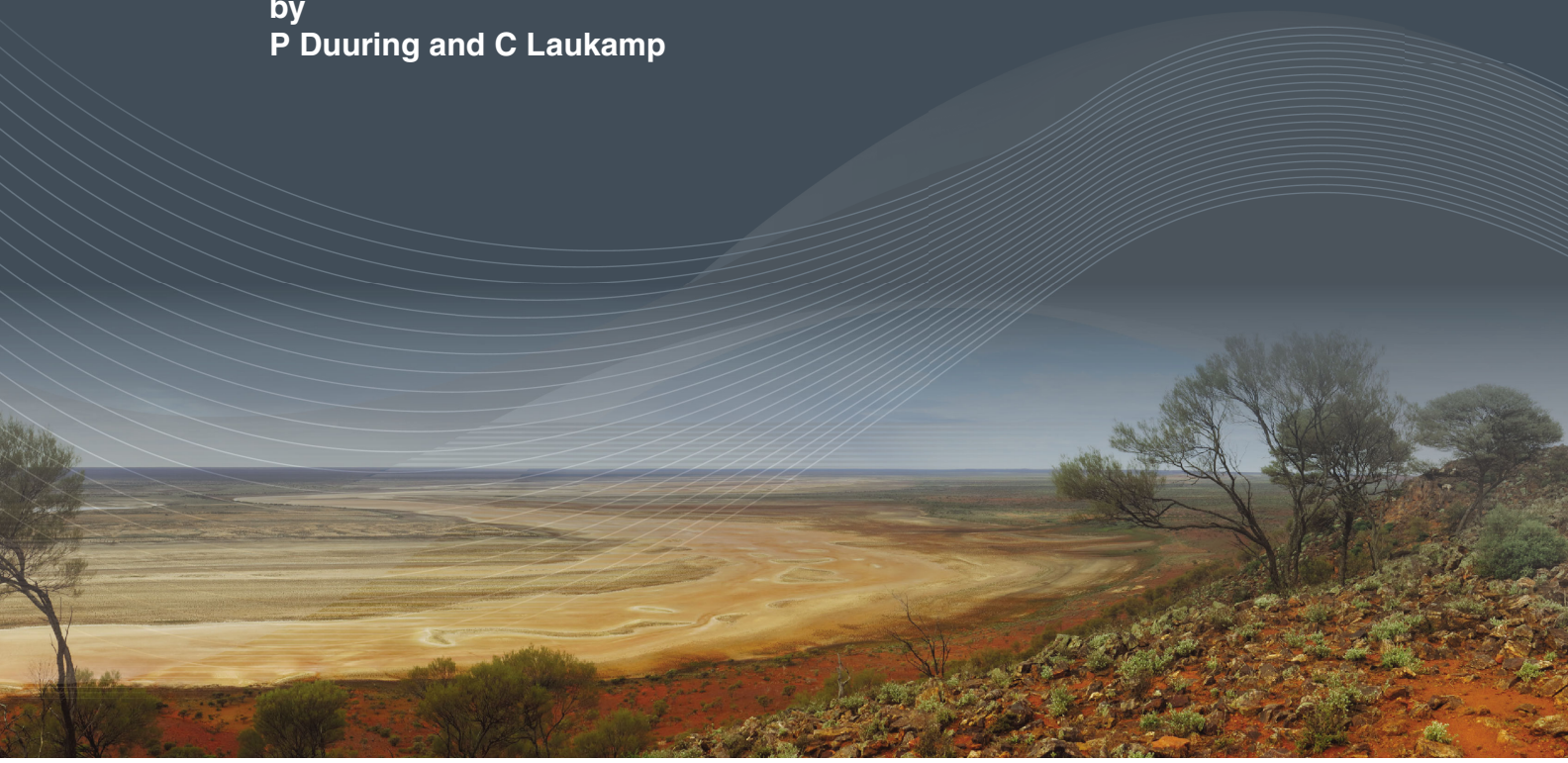

Geological Survey of Western Australia

EXPLORATION INCENTIVE SCHEME

Centre for EXPLORATION TARGETING

CSIRO

Government of **Western Australia**
Department of **Mines and Petroleum**

Record 2016/16

MAPPING IRON ORE ALTERATION PATTERNS IN BANDED IRON-FORMATION USING HYPERSPECTRAL DATA: BEEBYN DEPOSIT, YILGARN CRATON, WESTERN AUSTRALIA

by
P Duuring and C Laukamp[1]

1 Western Australian Centre of Excellence for 3D Mineral Mapping, CSIRO Mineral Resources, 26 Dick Perry Avenue, Kensington WA 6151

Perth 2016

Geological Survey of Western Australia

REFERENCE
The recommended reference for this publication is:
Duuring, P and Laukamp, C 2016, Mapping iron ore alteration patterns in banded iron-formation using hyperspectral data: Beebyn deposit, Yilgarn Craton, Western Australia: Geological Survey of Western Australia, Record 2016/16, 18p.

National Library of Australia Card Number and ISBN 978-1-74168--719-4

Grid references in this publication refer to the Geocentric Datum of Australia 1994 (GDA94). Locations mentioned in the text are referenced using Map Grid Australia (MGA) coordinates, Zone 51. All locations are quoted to at least the nearest 100 m.

Published 2016 by Geological Survey of Western Australia
This Record is published in digital format (PDF) and is available online at <www.dmp.wa.gov.au/GSWApublications>.

Further details of geological products and maps produced by the Geological Survey of Western Australia are available from:
Information Centre
Department of Mines and Petroleum
100 Plain Street
EAST PERTH WESTERN AUSTRALIA 6004
Telephone: +61 8 9222 3459 Facsimile: +61 8 9222 3444
www.dmp.wa.gov.au/GSWApublications

Cover image: Elongate salt lake on the Yilgarn Craton — part of the Moore–Monger paleovalley — here viewed from the top of Wownaminya Hill, 20 km southeast of Yalgoo, Murchison Goldfields. Photograph taken by I Zibra for the Geological Survey of Western Australia

Contents

Appendix

Figures

Mapping iron ore alteration patterns in banded iron-formation using hyperspectral data: Beebyn deposit, Yilgarn Craton, Western Australia

by

P Duuring and C Laukamp[1]

Abstract

Diamond drillhole WRRD0583, intersecting the W9 prospect of the Beebyn deposit in the Weld Range iron camp, was scanned with the GSWA HyLogger-3 at the Perth core library. The aim was to identify key hypogene and supergene alteration minerals associated with high-grade iron ore in banded iron-formation (BIF) and adjacent mafic igneous country rocks. BIF and mafic igneous rocks are best distinguished using the 'opaque mineral abundance' geoscience product, which maps the abundance of opaque minerals such as magnetite. High-grade hypogene magnetite–martite ore zones in BIF are accurately identified using the 'opaques abundance' and 'quartz abundance' products. A high ratio for opaques abundance vs quartz abundance corresponds to magnetite-rich, quartz-poor, high-grade iron ore zones. This index is more robust in BIF systems than the 'ferric iron to silica index', which is influenced by the oxidation state of the BIF rather than simply the iron content. High-grade, supergene goethite–hematite ore zones in BIF are identified by their high goethite/hematite ratio and corresponding low quartz abundance signatures. Proximal hypogene alteration zones in mafic igneous rocks are readily identified by an increase in the detected abundance of hydrothermal chlorite, with matching depletions in the detected abundances of igneous amphibole, plagioclase, and metamorphic epidote.

KEYWORDS: banded iron-formation, hypogene deposits, iron ores, spectral analysis, supergene alteration

Introduction

High-grade (>57 wt% Fe) iron ore deposits hosted by banded iron-formation (BIF) in the Yilgarn Craton of Western Australia are the product of early alteration by deeply derived hypogene fluids and later modification by near-surface supergene fluids (e.g. Koolyanobbing and Windarling deposits [Angerer and Hagemann, 2010]; Weld Range deposits [Duuring and Hagemann, 2013]; Jack Hills deposits [Maskell et al., 2014]). These deposits comprise near-surface, supergene, goethite–hematite orebodies that overlie deeper occurrences of hypogene magnetite and crystalline hematite ore. Importantly for iron ore exploration, hypogene orebodies are commonly enveloped by zones tens of metres wide of hypogene alteration minerals extending into unmineralized BIF and adjacent country rocks (e.g. at the Beebyn deposit; Duuring and Hagemann, 2013). However, closer to the present surface, hypogene alteration minerals are extensively replaced by supergene alteration minerals, and the resultant supergene-modified, hypogene alteration mineral patterns can be complex and difficult to decipher.

Recently, entire drillholes intersecting BIF and high-grade iron ore have been scanned for reflectance spectral data using the HyLogger-3 (e.g. the Channel Iron Deposits of the Rocklea Inlier, southern Pilbara region [Haest et al., 2012a]; martite–goethite ± microplaty hematite BIF-hosted ore at the Hashimoto deposit, Hamersley Basin [Gallagher, 2013]; martite–goethite-rich BIF-hosted iron ore at Mt Richardson, Yilgarn Craton [Chiarelli, 2015]). The advantage of such a system is the continuous high-resolution (1 cm) scan of diamond drillcore, which provides information about the distribution of alteration minerals and their mineral chemistry. The HyLogger-3 is particularly useful for distinguishing and quantifying iron oxide mineral species (e.g. hematite, goethite, and goethite subtypes), Al-clays (kaolinite, white mica, and smectite) and chlorite, which are common constituents of BIF-hosted iron systems (Haest et al., 2014).

1 Western Australian Centre of Excellence for 3D Mineral Mapping, CSIRO Mineral Resources, 26 Dick Perry Avenue, Kensington WA 6151

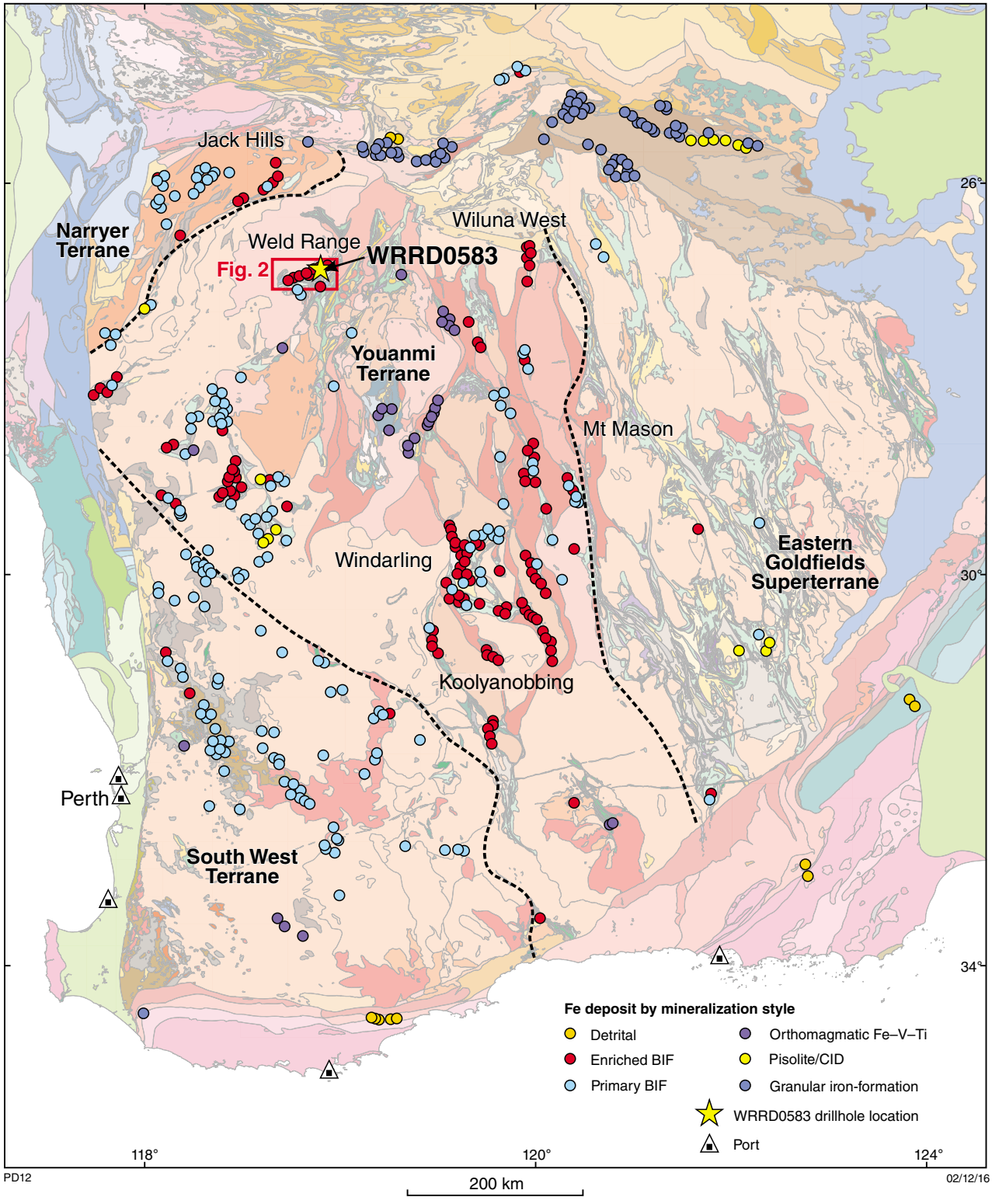

Figure 1. **Distribution of iron ore occurrences in the Yilgarn Craton and location of diamond drillhole WRRD0583 in the Weld Range iron camp. Regional geological map from GSWA (2016); iron ore deposits from the GSWA MINEDEX database <www.dmp.wa.gov.au/minedex>**

This study uses the HyLogger-3 to identify key hypogene and supergene alteration minerals that are associated with high-grade iron ore in BIF and surrounding unmineralized mafic country rocks at the Beebyn deposit in the Weld Range greenstone belt, Western Australia (Fig. 1). The goal is to help identify alteration mineral vectors to high-grade iron ore. The results from this study are also used to evaluate an existing interpretation of reflectance spectral data from satellite (e.g. ASTER) surveys of the Weld Range greenstone belt (Duuring et al., 2012).

Geological overview of the Beebyn deposit

The geological setting and characteristics of the Beebyn deposit, located within the Weld Range iron camp in the Murchison Domain of the Yilgarn Craton (Fig. 2), have been documented by Duuring and Hagemann (2013). Weathered BIF and mafic igneous rocks are exposed along an 8 km long, east-northeasterly trending ridge at the Beebyn deposit (Fig. 3). Three main BIF units (informally named the North, Central, and South BIF) are up to 80 m thick, trend east-northeast, and dip steeply (>80º) to the south-southeast. Basalt, dolerite, and gabbro country rocks envelop the North, Central, and South BIF (Fig. 4). All primary lithological contacts between BIF and mafic igneous rocks are deformed, with only thin (<3 m thick) dolerite sills within the three main BIF units recording primary intrusive contacts. Rare, <1 m thick, intervals of shale or siltstone are aligned parallel to bands within the North and Central BIF. A tectono-stratigraphic sequence is interpreted for the Beebyn deposit, with alternating silica- and Fe oxide-rich bands in the BIF units representing a composite of primary compositional layering and several transposed, fold- and shear zone-related, secondary fabrics (Duuring and Hagemann, 2013). The tectono-stratigraphic sequence is locally offset up to 200 m by north-northwesterly to north-northeasterly trending, subvertical faults (Fig. 2).

High-grade magnetite–martite (‘martite’ terminology after Clark, 1993) and near-surface goethite–hematite ore zones are thickest in the North BIF, coincident with the W11 and W10 prospects (Fig. 3). The adjacent prospects located to the west (W9, W8, W7) and east (W12) host narrower lenses of high-grade Fe ore. The Central and South BIF are also locally mineralized, but their ore zones are significantly thinner due, at least in part, to the narrower primary thickness of these host rocks. Surrounding mafic igneous rocks do not host high-grade Fe ore. The North BIF hosts high-grade Fe ore from the present surface to vertical depths of at least 250 m. Goethite–hematite ore zones in BIF extend from the surface to about 60 m depth, magnetite–martite-rich zones occur from 60 to 150 m, whereas magnetite-rich zones dominate in unweathered rocks below 150 m.

Below the weathering front, fresh BIF and nearby mafic igneous country rocks record multiple stages of structurally controlled, progressive hypogene alteration prior to the onset of near-surface weathering. These sequential hypogene alteration stages significantly affect the mineralogy, texture, and chemistry (including Fe content) of the least-altered BIF and mafic rocks. The result is a <80 m thick Fe orebody that displays zoned hypogene alteration mineral and geochemical patterns in BIF and mafic country rocks. The earliest hypogene alteration events (Stages 1 and 2; Duuring and Hagemann, 2013) affecting BIF involved the replacement of silica-rich bands by Stage 1 hypogene siderite and magnetite, followed by the addition of Stage 2 ferroan dolomite veins. These alteration events preserved the original texture of BIF, but changed the bulk chemistry of the BIF through a major depletion (98%) in the abundance of SiO_2, and increases in CaO, MgO, loss on ignition (LOI) content, C, P_2O_5, and $Fe_2O_{3(total)}$ (Duuring and Hagemann, 2013).

The Stage 3 hypogene alteration event involved the reactivation of existing structures and leaching of Stage 1 and 2 carbonate minerals. The removal of the carbonate gangue minerals and residual concentration of magnetite-rich bands produced high-grade, magnetite-rich ore zones in BIF that are thinly banded and locally crenulated, cavity rich, and brecciated. The ore zones are depleted in SiO_2 (by up to 99 %) and enriched in $Fe_2O_{3(total)}$, K_2O, CaO, MgO and P_2O_5 compared with least-altered BIF (Duuring and Hagemann, 2013).

Stage 4 chlorite–hematite ± talc hypogene alteration zones associated with 1 m wide, bedding-parallel shear zones locally replace least-altered and Stages 1, 2, and 3 altered BIF. Specular hematite lenses are locally present in the hinge areas of parasitic F_2 folds that deform the residual magnetite-rich ore zones. Stage 4 alteration zones and three more subsequent stages of hypogene alteration (i.e. Stages 5, 6 and 7; Duuring and Hagemann, 2013) involved the addition of SiO_2 to BIF. However, Stages 4 to 7 alteration zones have a restricted expression at the scale of the Beebyn deposit and are unlikely to have a major influence on the bulk chemistry of the orebody.

Fresh (i.e. unweathered) mafic igneous rocks also preserve a distinct hypogene alteration signature. Proximal and intermediate alteration zones located up to 20 m from the contact with BIF-hosted, magnetite-rich ore zones display replacement of primary and metamorphic Ca- and Na-rich minerals, such as amphibole, plagioclase and epidote, by hypogene ferroan chlorite, ferroan dolomite, and siderite. Geochemical anomalies include enrichments in LOI, MgO, and $Fe_2O_{3(total)}$ values, and depletions in SiO_2, CaO, K_2O, and Na_2O.

At the surface, hypogene-altered BIF displays a massive to mottled secondary texture caused by the destruction of mesobanding and the replacement of primary, metamorphic, and hypogene Fe oxides, silica-rich minerals, and carbonate minerals by fine-grained goethite. Supergene-altered mafic igneous rocks are fine grained and massive. Primary, metamorphic, and hydrothermal minerals are replaced by goethite, hematite, and kaolinite. Hematite is the dominant Fe oxide in supergene-altered mafic igneous rocks within 10 m of contacts with BIF, whereas goethite and kaolinite are dominant in more distal areas.

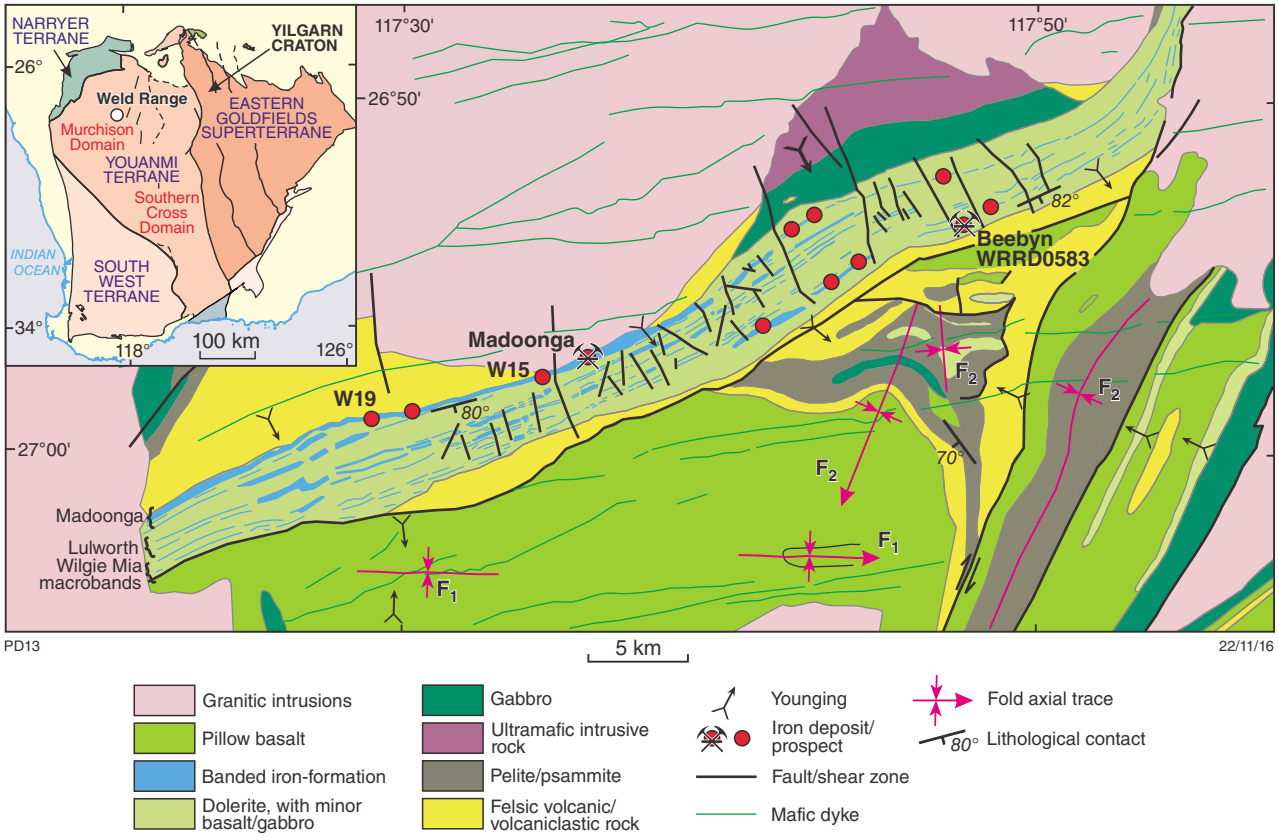

Figure 2. Regional solid geology map for the Weld Range iron camp (modified after Duuring and Hagemann, 2013), with location of Beebyn drillhole WRRD0583

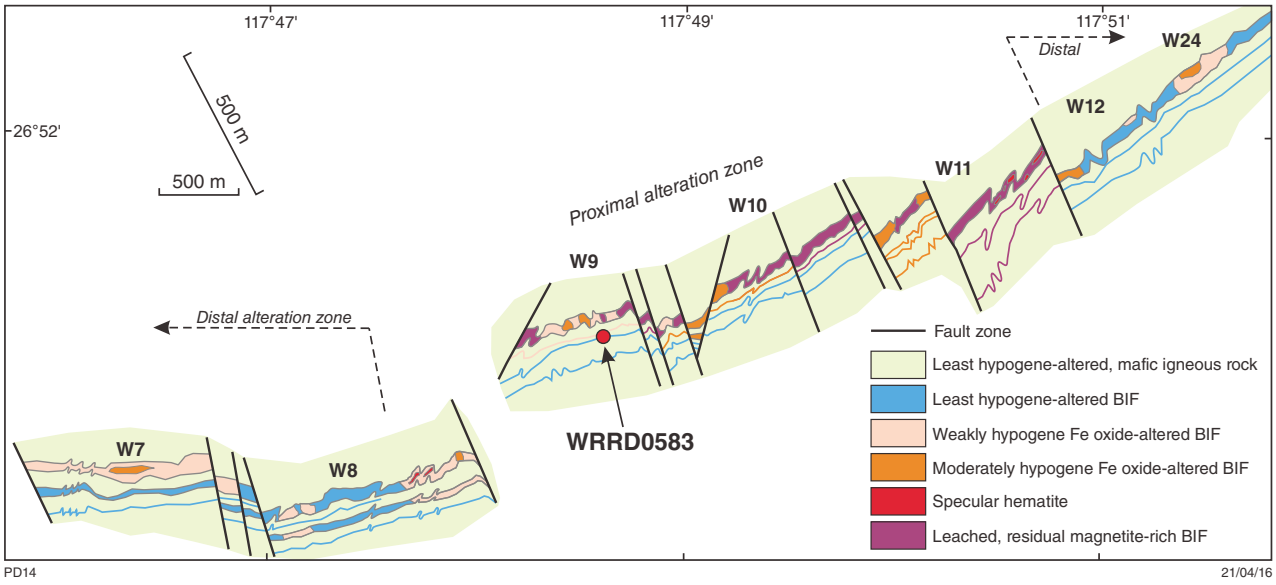

Figure 3. Location of drillhole WRRD0583 in the W9 prospect of the Beebyn deposit. Hypogene alteration zones in BIF are displayed in plan view (modified after Duuring and Hagemann, 2013). Note different scales in east–west and north–south directions

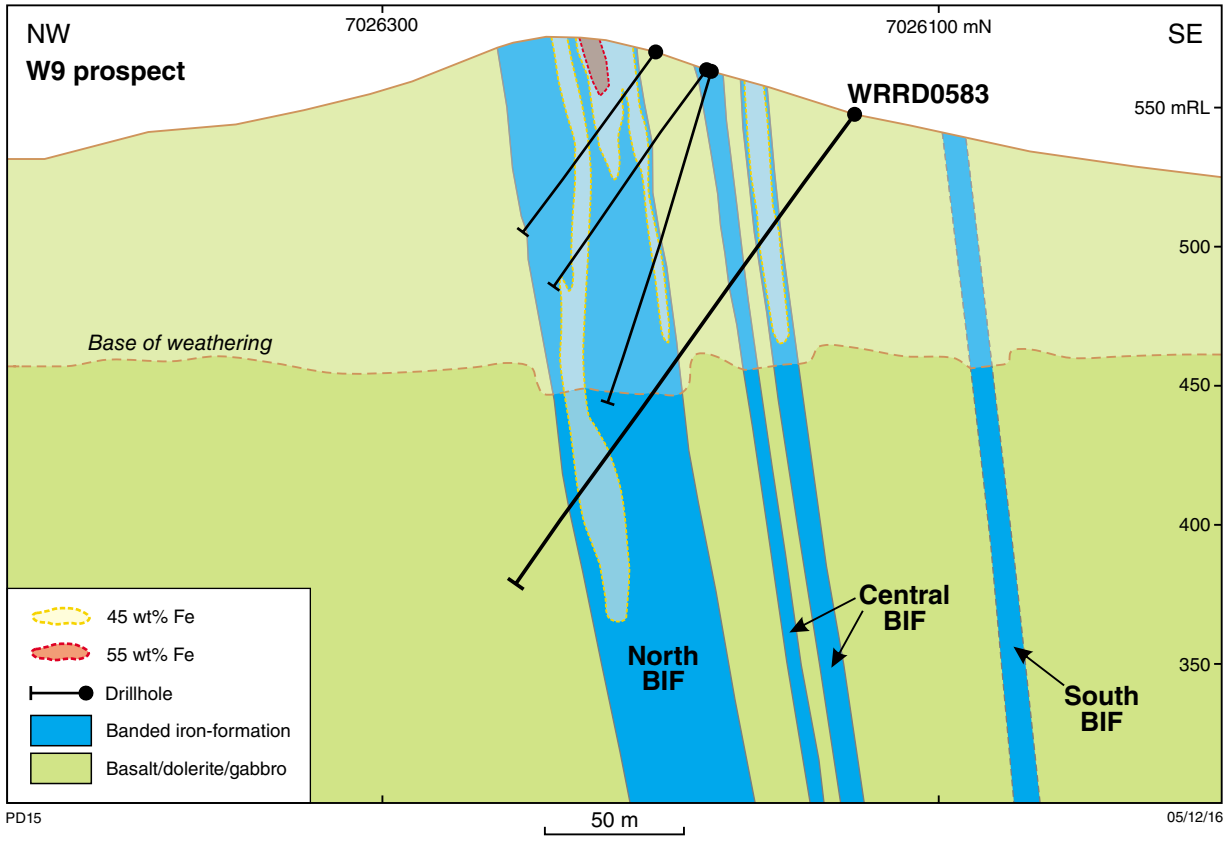

Figure 4. Cross-section through the W9 prospect, showing the location of drillhole WRRD0583 and the intersection of major rock types by the drillhole (modified after Duuring and Hagemann, 2013)

The most robust geochemical vector for supergene-modified, high-grade iron ore at the surface is the ratio of $Fe_2O_{3(total)}$ to SiO_2 content in rocks. Supergene alteration preserves or increases the $Fe_2O_{3(total)}/SiO_2$ ratio for BIF due to the addition of goethite or the pseudomorphic replacement of magnetite, hematite, silicate and carbonate minerals by goethite.

Results from the conventional logging of diamond drillhole WRRD0583

Diamond drillhole WRRD0583 is positioned in the Beebyn W9 prospect (MGA 580147E 7026132 N) and was drilled from the surface at an inclination of –55° towards 348° for 208.7 m (Figs 3, 4). Core from this hole was chosen for scanning by the HyLogger because it intersects examples of high-grade supergene goethite–martite ore (57–62 wt% Fe), as well as fresh, hypogene magnetite–martite ore (57–65 wt% Fe) in BIF. Fresh BIF displays visible changes in the abundance of hydrothermal carbonate minerals, and the ratio of primary silica-rich to iron oxide-rich bands, with proximity to hypogene magnetite–martite ore zones. Fresh mafic igneous rocks are enriched in chlorite within 15 m of the contact with BIF-hosted high-grade hypogene ore. Unless otherwise stated, depth measurements are in reference to the depth down the inclined hole rather than vertical depths from the present surface.

Core from drillhole WRRD0583 was transported from the Weld Range exploration camp to the Geological Survey of Western Australia's (GSWA) Perth Core Library in Carlisle in February 2014, where the core was cleaned, dried, and scanned with the HyLogger-3 by GSWA personnel. The diamond drillcore was logged by conventional means, which included the documentation of relationships between rock types, textures, structures, and hypogene and supergene alteration mineral assemblages, and comparison with bulk-rock geochemical data. Drillhole WRRD0583 was returned to the Weld Range exploration camp in April 2014.

Rock types

The 68 m thick North BIF and two macrobands of the Central BIF (6 and 14 m thick) are intersected by drillhole WRRD0585 (Fig. 4). The macrobands are separated by 8–28 m thick, dolerite and gabbro intrusions, whereas narrower dolerite dykes (1–10 cm thick) locally cut BIF mesobands (Fig. 5). Intense weathering extends from the surface to a depth of about 116 m and affects mafic igneous rocks, the Central BIF macrobands, and the upper 10 m of the North BIF. Deeper than about 116 m, the

North BIF displays a weak supergene overprint, whereas the underlying mafic igneous rocks from 172 m are fresh (Fig. 5).

Hypogene alteration of BIF

A 9 m thick, high-grade, hypogene magnetite–martite ore zone is located along the lower margin of the North BIF at depths from 160–169 m (Fig. 5). With proximity to the high-grade ore zone (i.e. from 147–160 m), primary silica-rich bands in the North BIF are progressively replaced by hypogene siderite and ferroan dolomite, with minor apatite. Over the same depth interval, SiO_2 decreases dramatically (from 60 to 2 wt%), with corresponding enrichments in P (from 0.018 to 0.150 wt%), LOI content (from 1 to 8 wt%), MgO (from 0.02 to 3.00 wt%), and CaO (from 0.01 to 0.50 wt%). Total Fe values do not change markedly owing to the direct substitution of primary quartz bands by hypogene siderite and ferroan dolomite. This hypogene alteration zone is hereby termed the 'outer' carbonate alteration zone in the North BIF.

The 'inner' high-grade, hypogene magnetite–martite ore zone in the North BIF (from 160–169 m) is characterized by the removal of hypogene siderite and ferroan dolomite. The inner alteration zones are enriched in primary iron oxide bands owing to the dissolution of the carbonate minerals. The resultant rock is thinly banded and displays a schistosity that increases in intensity towards the lower contact of the North BIF at about 170 m. Disseminated, euhedral hypogene magnetite overprints primary iron oxide bands and constitutes up to 20 vol% of the rock. The inner alteration zone displays an enrichment in total Fe (from 45 to 65 wt%), with a corresponding decrease in P (from 0.261 to 0.084 wt%), LOI content (from 12 to 5 wt%), and MgO (from 5.00 to 0.65 wt%).

Hypogene alteration of mafic igneous rocks

Fresh, mafic igneous rocks located along the lower margin of the North BIF increase in grain size with depth, from dolerite (at 172–186 m) to gabbro (186 – 208.7 m) located at the bottom of the hole. It is unclear if this grain size variation represents different generations of mafic intrusions, a chilled contact between the gabbro and BIF, or if it is one gabbro unit that has experienced intense hypogene chlorite alteration along the contact with BIF.

Dolerite located proximal to the BIF-hosted magnetite–martite ore zones (i.e. 172–176 m) is fine grained, massive, weakly schistose, and chlorite rich, with minor carbonate minerals and possibly talc. Primary igneous amphibole and plagioclase are replaced by metamorphic epidote, followed by hydrothermal chlorite. Dolerite located in 'intermediate' zones (i.e. 176–183 m) is altered to hydrothermal chlorite, but with a higher abundance of igneous amphibole and plagioclase. Distal alteration areas in dolerite (183–186 m) comprise weak hypogene chlorite and a greater abundance of igneous amphibole and plagioclase, with metamorphic epidote.

Gabbro in the interval 186 – 208.7 m is coarse grained and massive, and consists of amphibole and plagioclase, with minor metamorphic epidote and chlorite. Narrow quartz–carbonate veins and wallrock alteration haloes are common from 183 to 202 m. With proximity to BIF-hosted hypogene magnetite–martite ore zones, fine-grained mafic igneous rocks demonstrated an increase in MgO (from 5 to 9 wt%) and a corresponding decrease in CaO (from 13.0 to 0.2 wt%) and K_2O (from 1.5 to 0.4 wt%).

Supergene alteration of BIF

The two Central BIF macrobands are intensely supergene altered and comprise mainly goethite and hematite. The intensity of supergene goethite–hematite increases towards the base of each BIF macroband, corresponding to the location of 1–2 m wide, fault zones (Fig. 5).

Supergene-altered BIF displays dissolution or replacement of primary silica-rich bands by ochreous and vitreous goethite; in some areas the dissolution of quartz results in a high secondary porosity in the rock. Primary iron oxide-rich bands are mostly replaced by supergene martite and goethite. Relative to fresh, least-altered BIF, supergene alteration results in a dramatic decrease in SiO_2 (from 46 to 2 wt%), with a matching increase in Fe (from 36 to 62 wt%), P (from 0.017 to 0.143 wt%), LOI content (from 0.63 to 7.00 wt%), and a local increase in Mn (<0.7 wt%). Minor (<5 vol%) disseminated hypogene magnetite (now martite) replaces primary bands in the Central BIF. Magnetic susceptibility data available for this interval demonstrates demagnetization of the primary BIF due to the replacement of primary and hypogene magnetite by supergene goethite and hematite (Fig. 5).

Supergene alteration of mafic igneous rocks

Intense supergene alteration is exhibited by dolerite and gabbro to a depth of 20 m from the present-day surface. In this interval, primary igneous amphibole, pyroxene, olivine, and plagioclase, and metamorphic epidote and chlorite, are replaced by goethite (ochreous and vitreous), cryptocrystalline hematite, and kaolinite. Moderate supergene alteration extends to depths of about 120 m, with localized zones of more intense supergene alteration occurring in mafic igneous rocks within 10 m of contacts with BIF (e.g. from 35 to 45 m depth; Fig. 5). Supergene cryptocrystalline hematite is more abundant than goethite within 20 m of the surface and in proximal areas to BIF contacts. Relative to fresh mafic igneous rocks, intensely supergene-altered rocks are enriched in LOI content (from 4 to 8 wt%) and depleted in MgO (from 10.0 to 0.1 wt%), CaO (from 1.80 to 0.02 wt%), K_2O (from 0.43 to 0.02 wt%), and Na_2O (from 1.90 to 0.02 wt%). Gamma radiation data for dolerite and gabbro demonstrates a higher radioactivity associated with the freshest examples of these rocks (Fig. 5).

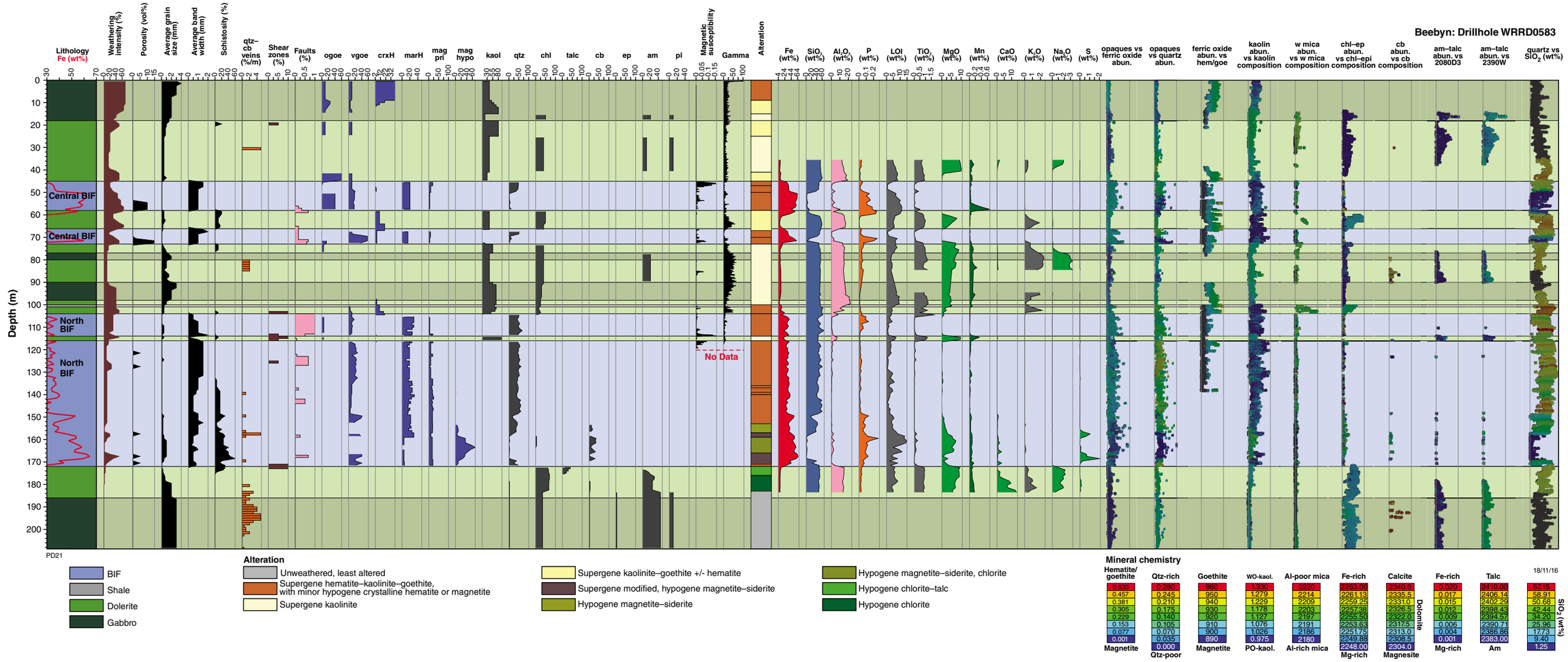

Figure 5. Hyperspectral log for WRRD0583. Abbreviations: abun – abundance; am – amphibole; cb – carbonate; chl – chlorite; crxH – crystalline hematite; ep – epidote; ferric oxide – ferric oxide minerals; kaol – kaolinite; mag hypo – hypogene magnetite; mag pri – primary magnetite; marH – martite; ogoe – ochreous goethite; opaques – opaque minerals; pl – plagioclase; PO-kaol – poorly ordered kaolinite; qtz – quartz; vgoe – vitreous goethite; w mica – white mica; WO-kaol – well-ordered kaolinite

Results of hyperspectral data acquisition and processing

Method

The HyLogger-3 hyperspectral scanning system developed by CSIRO in Australia uses reflectance spectra of scanned diamond drillcore to identify mineral abundances and mineral chemistry (Hunt, 1977; Clark and Roush, 1984). The HyLogger-3 operated by GSWA in Perth detects radiation reflected from the drillcore within the visible to near infrared (VNIR, 380–1000 nm), short wave infrared (SWIR, 1000–2500 nm) and thermal infrared (TIR, 6000–14000 nm) parts of the electromagnetic spectrum. The HyLogger-3 uses an automated x–y table that moves the core tray at intervals of 1 cm data resolution (Haest et al., 2012a). The reflectance spectra are cross-calibrated using a Spectralon panel. During the nondestructive scanning process, the HyLogger-3 also captures high-resolution digital core images, which are referenced to a standard set of Munsell colours. The hyperspectral data are then processed to determine the abundance of minerals, as well as their composition and/or crystallinity, based on the wavelength, depth and width of diagnostic absorption features. Algorithms applied in this project were developed by CSIRO (Laukamp, 2011; Haest et al., 2012b; Sonntag et al., 2012) and were used in this study to determine mineral abundance and composition of iron oxides, including hematite, vitreous goethite and ochreous goethite, and other minerals such as chlorites, carbonates, amphiboles, white micas, and kaolin group minerals (Appendix 1).

The collected VNIR, SWIR, and TIR spectral signatures were processed using the commercial software The Spectral Geologist (TSG). Mineral abundance and composition information were extracted using the multiple feature extraction method (Cudahy et al., 2008; Laukamp et al., 2010). Positions and depths of absorption features in this study were calculated by locally removing the hull from the reflectance spectra to reduce the influence of instrument or atmospheric noise (Cudahy et al., 2008).

The use of mineralogical diagnostic absorption features allows the identification of the mineralogy, although quantitative determination of this mineralogy is often more difficult (Clark and Roush, 1984). Iron oxides produce diagnostic absorption features in the VNIR, which are caused by electronic processes involving Fe^{3+} cations octahedrally bonded to ligands of oxygen (hematite, αFe_2O_3) or oxygen and hydroxyl (goethite, αFeOOH) (Cudahy and Ramanaidou, 1997). These electronic processes include the transfer of electrons within electron orbits or from ligand to metal iron (i.e. charge transfer). Energy of absorption processes can be altered by changes in valence state, coordination number, site symmetry, type of ligand, distortion of metal–ligand site, the length of the metal–ligand distance, and mineral properties (grain size, shape, orientation, density, matrix, and temperature) (Adams and Filice, 1967; Sherman et al., 1982; Singer and Roush, 1985).

In major rock-forming minerals, such as hydrated silicates, diagnostic absorption features are located in the SWIR, which are related to the overtones of fundamental stretching vibrations, and a combination of fundamental stretching and bending vibrations of the hydroxyl group. Two types of geoscience information products were generated to characterize the 'mineral abundance' and 'mineral composition'. The method for generating these two types of products uses the relative band depth for mineral abundance and the wavelength position of a mineral-specific absorption feature for the mineral composition. The depth and shape of mineral-related absorption features in the visible to near and short wave infrared are directly related to the physicochemistry of the investigated material and can be captured from spectral data using band ratios. In the TIR wavelength range, the spectral signature is, in addition to the mineral physicochemistry, strongly influenced by grain size, emissivity, and optical properties (e.g. surface vs volume scattering).

For this study, emphasis was given to reflectance spectral geoscience products that indicate the presence of Fe ore zones in BIF, and tests for alteration minerals in BIF and neighbouring basalt or dolerite country rocks. These products include: 1) 'opaque' minerals (e.g. magnetite and pyrite); 2) 'ferric oxide' minerals (e.g. hematite and goethite); 3) 'kaolinite composition' (e.g. well-crystalline vs poorly crystalline); 4) 'white mica' minerals (e.g. Al rich and Al poor); 5) 'ferrous iron in silicate or carbonate' minerals (e.g. actinolite, chlorite, and siderite); 6) 'carbonate' minerals (e.g. calcite, dolomite, and magnesite). Quartz abundance is measured using the TIR bands. In all reflectance spectral data products, the relative abundance of minerals is indicated by the distribution of the data with vertical depth down the drillhole. The horizontal axes for these plots are without units. In most plots, the mineral abundance data are coloured based on mineral composition.

Rock types

BIF is best distinguished from mafic igneous rocks using the opaque mineral abundance spectral product, which detects the abundance of primary magnetite-rich bands in BIF. In contrast, mafic igneous rocks display a weak spectral signature for opaque minerals because of the minor presence of disseminated igneous magnetite (Figs 5, 6a). Dolerite and gabbro mostly display higher chlorite, chlorite–epidote, amphibole–talc, and plagioclase abundance spectral signatures relative to BIF (Fig. 5); however, these signatures vary widely depending on the local effects of weathering and differences in protolith compositions. In addition, the quartz abundance signature is generally highest for BIF (Fig. 5), but varies depending on hypogene and supergene alteration intensities (i.e. supergene and hypogene alteration results in lower detected quartz abundance values for BIF). Dolerite and gabbro display lower quartz abundance signatures than BIF, apart from areas of later quartz–carbonate veins and associated hypogene alteration; for example, within 15 m of contacts with BIF (Figs 5, 6b).

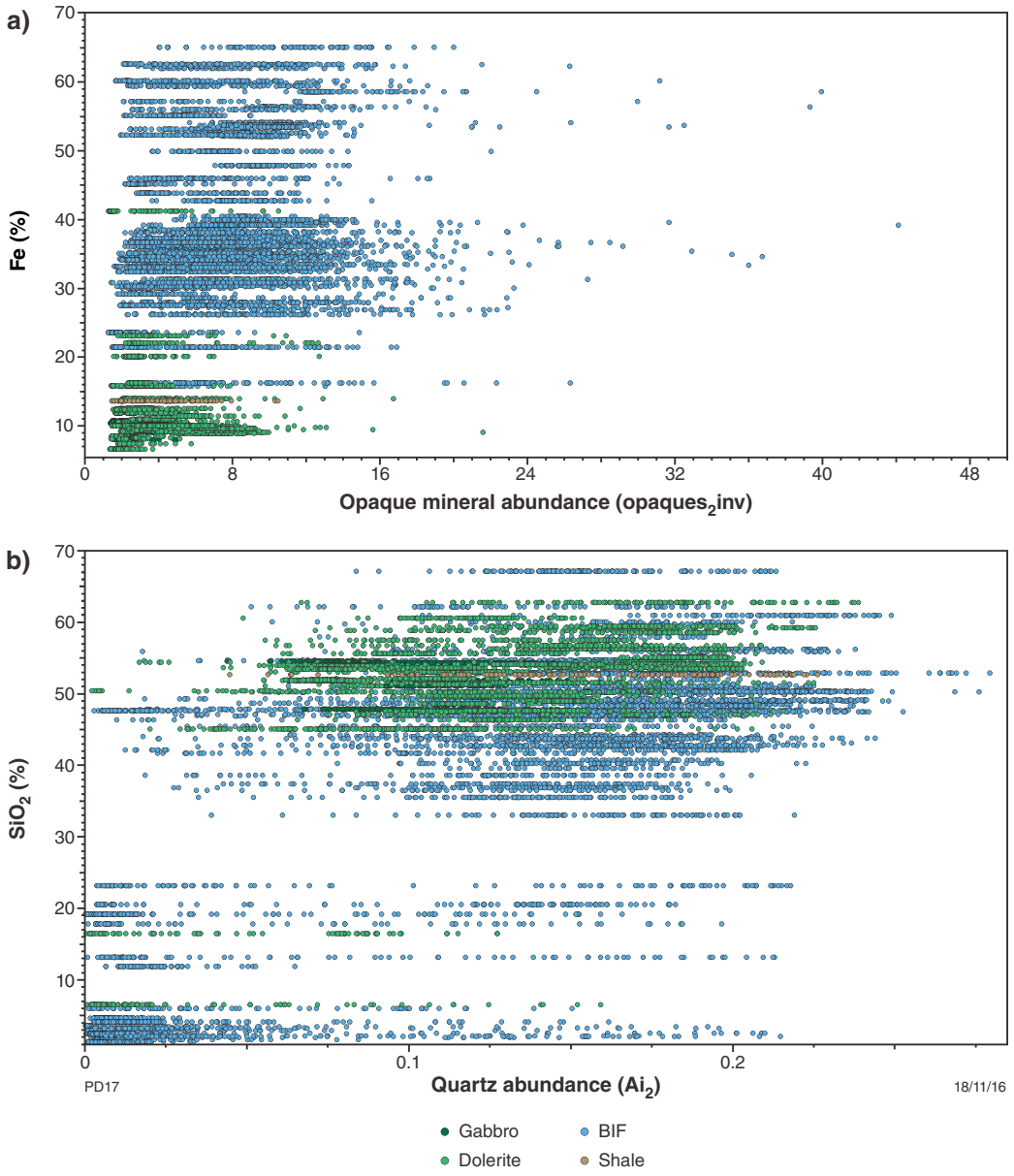

Figure 6. **Scatter plots from hyperspectral data for BIF and mafic rock: a) abundance of Fe detected from bulk-rock geochemical analysis vs opaque mineral abundance; b) SiO_2 content from bulk-rock geochemical analysis vs quartz abundance. Rocks generally display positive correlations in both plots. The broad variations in hyperspectral data are in part the result of sample interval differences between collected spectral data (1 cm intervals) vs the 1 m sampling interval for bulk-rock geochemical analysis.**

Dolerite and gabbro intrude the Central and North BIF macrobands at various depths in the diamond drillhole. Relative timing relationships are not displayed by individual mafic igneous intrusions and, apart from grain size differences, it is difficult to distinguish these units based on their petrological characteristics. Whole-rock geochemical data are available for these rocks for part of the diamond drillhole; specifically, over a sampling interval within 10 m of contacts with BIF, and continuously between the Central and North BIF macrobands (Fig. 6). Based on immobile element ratios (Al_2O_3 vs TiO_2), it is possible to separate the dolerite and gabbro into different compositional groups that reflect protolith chemistry (Figs 5, 7a). Hyperspectral data can also be used to separate the dolerite and gabbro into at least three compositional groups based on the Fe/Mg ratio for amphiboles (Figs 5, 7b). Based on thin-section observations, these amphiboles are primary igneous in origin and have only experienced lower greenschist facies metamorphic conditions, with local replacement by metamorphic epidote and chlorite. Hyperspectral data show that Fe-rich amphiboles are more common in dolerite located beneath the North BIF near the bottom of the drillhole (178–185 m), whereas Mg-rich amphiboles are dominant above the North BIF in the upper 120 m of the hole (Figs 5, 7c). These measured differences in amphibole chemistry relative to sample depth in dolerite also persist in gabbro (Fig. 7b,c), which is consistent with the dolerite representing the finer grained chilled contacts of gabbro intrusions.

Outer hypogene alteration zones in BIF

Relative to least-altered BIF, the outer carbonate-rich alteration halo to high-grade hypogene magnetite–martite ore zone in the North BIF (i.e. from 147 to 160 m) is characterized by: 1) a decrease in quartz abundance; 2) an increase in dolomite abundance; 3) a decrease in ferric oxide mineral abundance; 4) an enrichment in Fe-rich chlorite (Fig. 5). These mineral abundance and chemistry trends correspond to the replacement of primary silica-rich bands in BIF by hypogene siderite and dolomite (magnesite was not previously detected). The decrease in ferric oxide mineral abundance relates to the decrease in intensity of supergene alteration with depth (i.e. decrease in goethite and hematite), whereas localized enrichments in Fe-rich chlorite (Fig. 8a) coincide with the presence of narrow chlorite and amphibole-rich dykes in BIF.

Inner high-grade hypogene alteration zones in BIF

The high-grade hypogene magnetite–martite ore zone located at depths of 160–169 m in the North BIF coincides with a dramatic decrease in quartz abundance and a more subtle increase in opaque mineral abundance, relative to less-mineralized BIF. A local peak in the abundance of opaque minerals at 163 m accurately correlates with a mapped zone of intense, disseminated, hypogene magnetite alteration and low abundances of silica and carbonate gangue minerals in BIF.

The opaque mineral abundance index coloured by ferric oxide mineral abundance (indicating magnetite vs hematite or goethite abundance) identifies the magnetite-rich zone at 159–165 m (indicated by the dark blue circles in the respective plot in Fig. 5). Bordering areas are also magnetite rich, but display a hematite and goethite overprint associated with supergene alteration (e.g. at 165–172 m). These identified supergene-altered zones include narrower (1 m wide) zones at 166.6 m and 170.0 m that are enriched in hematite relative to goethite (indicated by the ferric oxide mineral abundance product coloured by hematite vs goethite in Fig. 5). These hematite-rich zones coincide with fault zones that host hypogene specular hematite overprinted by supergene goethite.

The broad zones of goethite in the high-grade, magnetite-rich zone, indicated by the warm colours shown in the ferric oxide abundance vs hematite/goethite geoscience product from 157–165 m (Fig. 5), are most likely the result the partial replacement of hypogene siderite and dolomite by goethite.

Rare amphibole and Fe-rich chlorite detected by the SWIR spectrometer at 160 m corresponds with 1–30 cm thick, fine-grained dolerite dykes that cut the high-grade ore zone.

Hypogene alteration zones in mafic igneous rocks

Fresh dolerite located along the lower contact of the North BIF is divided into proximal, intermediate and distal hypogene alteration zones relative to high-grade magnetite-rich ore zones in BIF. Proximal alteration zones (172–176 m) are rich in chlorite, with primary amphiboles and plagioclase completely replaced in this zone. These zones are fresh with no kaolinite present. Contrary to observations from conventional logging, talc was not detected in proximal zones by the SWIR spectrometer (i.e. the amphibole–talc abundance vs 2080D3 product demonstrates the presence of amphibole only). Intermediate alteration zones (176–183 m) contain chlorite, with primary amphibole and plagioclase, and metamorphic epidote, detected. Distal alteration zones in dolerite located from 183–186 m show a decrease in the abundance of chlorite and a corresponding increase in primary amphibole and plagioclase. Gabbro located from 186 m to the bottom of the hole displays consistent enrichments in chlorite, amphibole, pyroxene and epidote, with the exception of an interval of calcite–quartz veins from 187–200 m (Fig. 6). The quartz abundance signature increases in mafic igneous rocks with proximity to BIF contacts (Fig. 5).

Apart from the greater abundance of chlorite in proximal (and intermediate) alteration zones, there are no significant differences in the composition of chlorite with proximity to BIF-hosted magnetite-rich ore zones (Fig. 8b). Rather, the range in chlorite composition appears to be controlled by primary compositional differences in rock type, whereby Mg-rich chlorite is associated with dolerite and Fe-Mg chlorite is associated with gabbro at deeper intervals in the hole (Fig. 9). Interestingly, similar

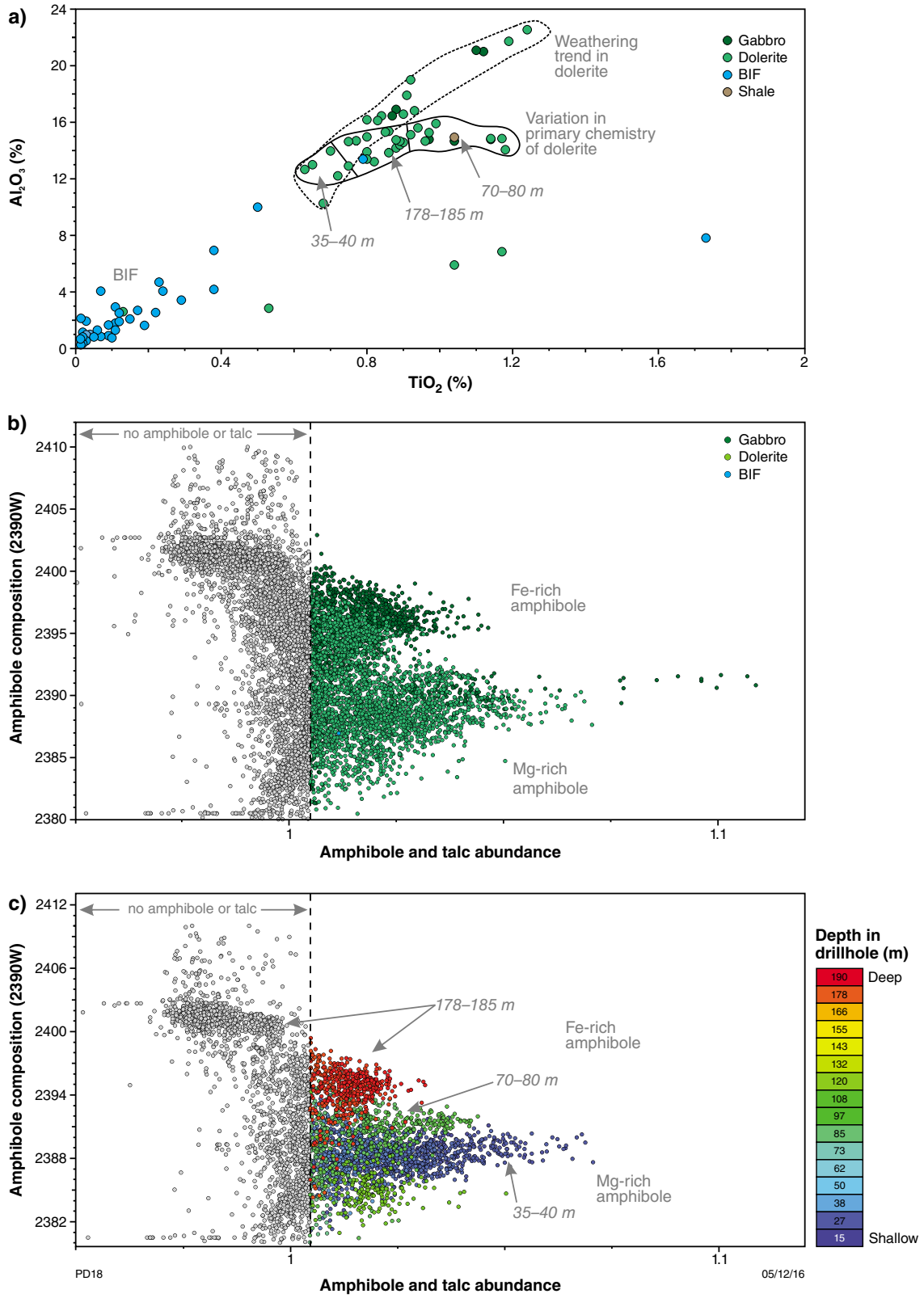

Figure 7. **Bulk-rock chemistry and amphibole chemistry for mafic igneous country rocks: a) immobile elements (TiO_2 [wt%] vs Al_2O_3 [wt%]) for mafic igneous rocks demonstrate variations based on primary compositional differences and weathering intensity; b) amphibole composition vs amphibole and talc abundance by rock type. Amphibole compositions vary between Fe rich and Mg rich for gabbro and dolerite. Overlap of data for gabbro and dolerite suggests that petrological differences are due to (finer grained) dolerite representing the chilled margins of gabbro intrusions; c) amphibole composition vs amphibole and talc abundance by depth in drillhole. Amphibole compositions for dolerite define at least three clusters that relate to the position of the dolerite in the drillhole and its intrusive position relative to BIF.**

distributions in Fe/Mg contents of primary amphiboles were demonstrated for dolerite (Figs 5, 7c) and gabbro, suggesting that hydrothermal or metamorphic chlorite that replaces primary amphibole inherits the Fe/Mg signature of the parent amphibole.

Supergene alteration zones in BIF

Supergene alteration intensity in the Central BIF macrobands is indicated by a decrease in the quartz abundance index and a coincident increase in the ratio of goethite vs hematite (measured by the hematite/goethite index; Fig. 5). For example, moderately weathered (low- to medium-grade) BIF at 66–70 m depth comprises mostly magnetite–martite bands and displays a corresponding low goethite/hematite ratio. In contrast, intensely weathered (high-grade) BIF at 70–72 m is enriched in goethite (and kaolinite) owing to the replacement of primary silica-rich and magnetite–martite bands by these minerals (Fig. 5). Thus, a low quartz abundance signature and a coincident high goethite/hematite abundance signature are effective indicators for high-grade supergene iron ore in BIF.

Supergene alteration of mafic igneous rocks

Supergene alteration of mafic igneous rocks is most intense within 14 m of the surface. The intensity gradually decreases with depth, with local increases associated with the deformed contacts of BIF. From the surface to a depth of 14 m, intensely weathered mafic igneous rocks display a high abundance of ferric oxide minerals compared with underlying less-weathered rocks. These intensely weathered zones are enriched in hematite relative to goethite (Fig. 5) and they are rich in kaolinite but depleted in chlorite, amphibole, and talc.

Moderately supergene-altered mafic igneous rocks located from 14 to 40 m contain lower abundances of ferric oxide minerals, with goethite present in equal proportions to hematite. Al-poor white mica (phengite) is present in this zone. Kaolinite abundance displays an inverse relationship with the abundance of chlorite, amphibole, and minor plagioclase (Fig. 5). Chlorite and amphibole abundance varies depending on weathering intensity, hypogene alteration, and protolith compositions of dolerite (Fig. 5).

Approaching deformed contacts with BIF (i.e. within 10 m), mafic igneous rocks display an increase in weathering intensity. Relative to distal less-weathered rocks, these proximal zones are enriched in kaolinite and ferric oxide minerals, and display varying but approximately equal proportions of hematite and goethite (Fig. 5). Weathered mafic igneous rocks located proximal to high-grade goethite–hematite ore zones in BIF are depleted in chlorite within 2 m of the deformed contact. More distal zones are enriched in chlorite, probably owing to the weathering of hypogene or metamorphic chlorite in these rocks (e.g. at 60–65 m and 100–102 m). Mg-rich chlorite is dominant in the first 100 m of the drillhole, with the exception of narrow intervals of Fe–Mg chlorite at 60–65 m and approaching the upper contact of the North BIF at 99–102 m (Fig. 5). The cause of these local changes in chlorite composition is unclear, but it may be related to local changes in the protolith chemistry of the dolerite at these depths.

Discussion

Key findings for WRRD0583 and implications for exploration

Hyperspectral data for the diamond drillhole were evaluated by their comparison with conventional logging observations and bulk-rock geochemical data. The comparison of these datasets shows that hyperspectral data accurately map differences in rock types, mineral abundance, and mineral chemistry. The advantages of the HyLogger-3 over conventional core logging include: a greater density of data with higher spatial resolution; the ability to define ranges in mineral compositions for chlorite, amphibole, and kaolinite; and the evaluation of minerals that are difficult to discriminate by conventional means (e.g. talc vs kaolinite). Noted inaccuracies in trends (in Fig. 5) between Fe content vs opaque mineral abundance, or SiO_2 (%) vs quartz abundance, are the product of sampling interval disparity between bulk-rock geochemical data (collected over a 1 m interval) compared with hyperspectral data (representing 1 cm intervals). These inaccuracies are greatest for least-altered BIF, which display large compositional variations on a 1–3 cm scale due to their alternating iron oxide- and silica-rich bands.

A key finding of this study is that the opaque mineral abundance product was most accurate at distinguishing BIF from mafic igneous rocks, owing to the dominance of magnetite-rich primary bands in BIF. This product is effective in weakly to moderately supergene-altered rocks, where magnetite-rich bands are at least partly preserved. Consequently, this spectral product might be used as an effective primary filter to identify BIF occurrences within spectral datasets. After applying this filter, spectral data for BIF can be evaluated specifically for variations in mineral abundance and mineral chemistry associated with iron ore. The opaque mineral abundance product has previously been recognized as an effective discrimination tool for BIF exposures using ASTER image geoscience products for the Weld Range district (Duuring et al., 2012).

The quartz abundance product is an effective secondary filter for identifying high-grade iron ore zones in BIF. The product measures the dramatic decrease in quartz abundance associated with hypogene and supergene ores. Mafic igneous rocks commonly display lower quartz abundance signatures than BIF, with the exception of intervals containing late quartz veins and related hydrothermal alteration zones.

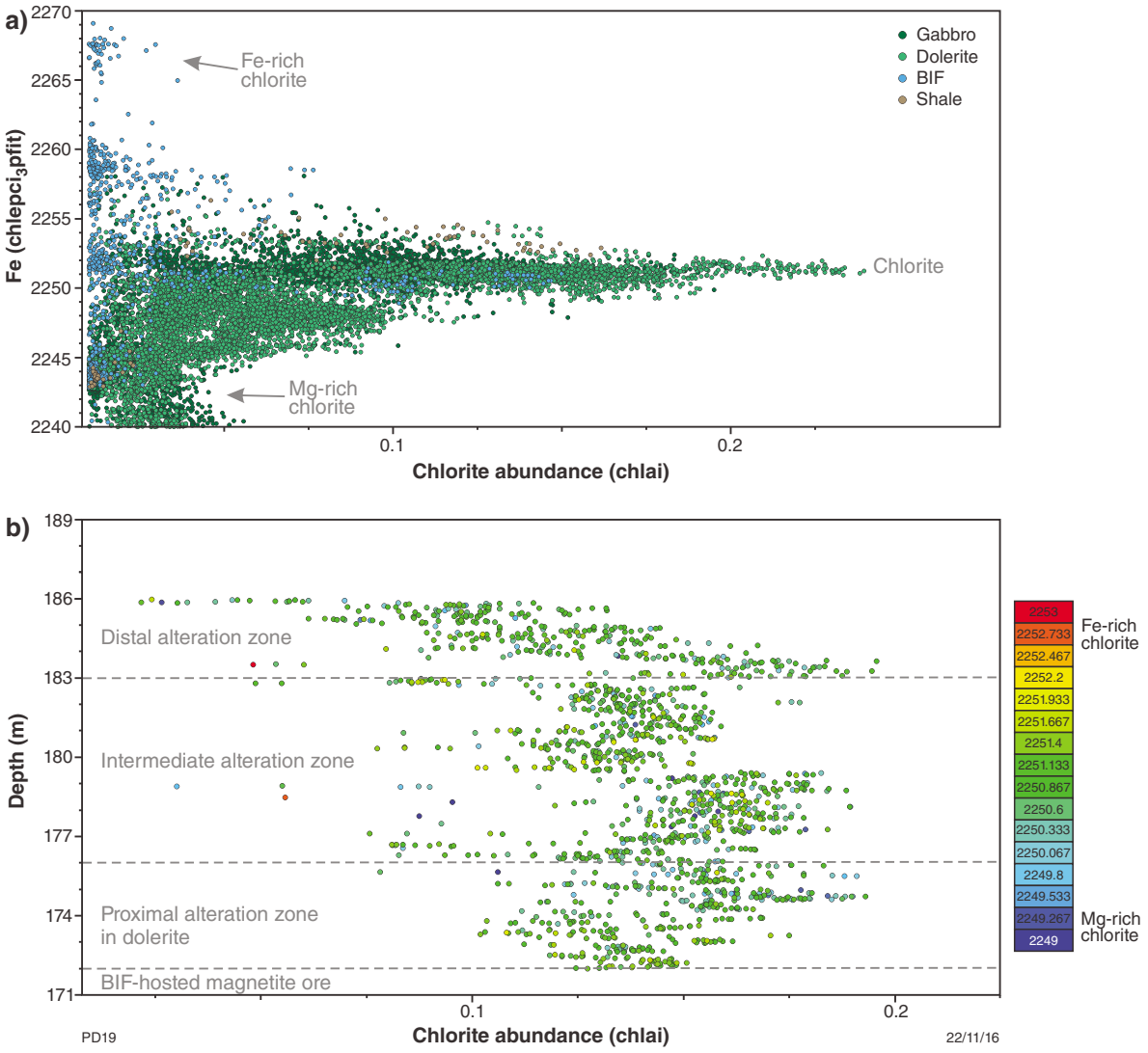

Figure 8. **Chlorite abundance and mineral chemistry trends interpreted from hyperspectral data: a) Fe content in chlorite vs chlorite abundance by rock type. Iron-rich chlorite is only detected in some intervals of BIF that are most likely associated with the occurrence of 1–30 cm thick, chlorite-rich mafic dykes. Distinct compositional groups in gabbro and dolerite correspond to the Fe/Mg ratio differences detected for primary amphibole; b) enlargement from Figure 5 of the depth interval from 171 to 186 m, corresponding to transition from proximal to distal alteration zones in dolerite. There is no discernible difference in Fe/Mg chemistry for chlorite with distance from the contact with BIF-hosted magnetite ore.**

The 'opaques to silica index' and the 'ferric iron to silica index' ASTER products have been successfully used to identify high-grade iron ore at Weld Range (Duuring et al., 2012). However, the results of this present study show that the ferric oxide abundance varies considerably in BIF and mafic igneous rocks depending on weathering intensity. Consequently, in some instances of intense weathering, BIF and mafic igneous rocks may have comparable signatures. Thus, the ferric iron to silica index is a less accurate indicator for iron ore than the opaques to silica index. This distinction between the two ASTER products explains the greater accuracy for the opaques to silica index in defining high-grade iron ores hosted by BIF at the Beebyn deposit (fig. 4b vs fig. 4c in Duuring et al., 2012). Note that silica abundance was used in preference to the quartz abundance product during the analysis of ASTER products by Duuring et al. (2012) because of the poor pixel resolution and discontinuous line striping effects associated with the quartz abundance ASTER product. The silica abundance product was not tested by the HyLogger-3.

Supergene goethite-rich hematite ore zones in BIF are identified by a decrease in quartz abundance and a corresponding increase in the ratio of goethite vs hematite (measured by the hematite/goethite index). These trends were consistently demonstrated by the two Central BIF macrobands. Consequently, the ratio of quartz abundance

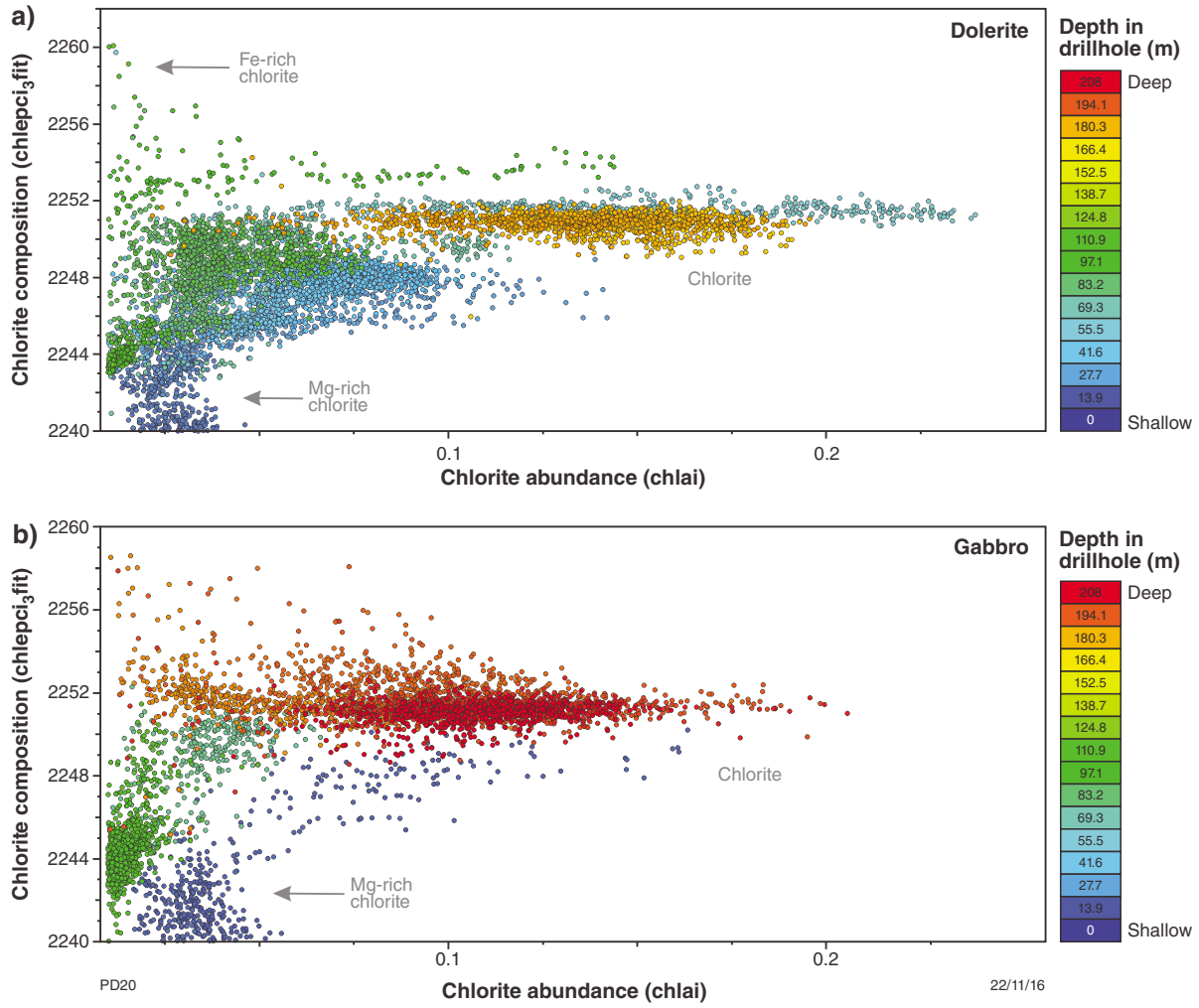

Figure 9. Chlorite abundance and mineral chemistry trends interpreted from hyperspectral data for dolerite and gabbro: a) dolerite contains chlorite that displays a broad range of Fe/Mg chemistry, including Fe-rich and Mg-rich end member compositions. Hypogene chlorite analysed at depths from 171 to 186 m (indicated by the orange circles) cannot be chemically distinguished from metamorphic chlorite located elsewhere in the drillhole; b) gabbro displays similar chlorite composition ranges as dolerite

vs the goethite index is an effective method for detecting high-grade supergene iron ores. This index could be used in addition to the established opaques to silica index, or the ferric iron to silica index, to identify iron ore (Duuring et al., 2012). It has the advantage over the opaques to silica index in that it identifies supergene goethite-rich ores rather than hypogene magnetite-rich ores.

Mafic igneous country rocks can be discriminated based on the compositional differences in their primary igneous amphiboles. Consequently, the hyperspectral amphibole chemistry product ('2390W'; Laukamp et al., 2012) is effective for mapping primary differences in the chemistry of mafic igneous rocks that are unweathered or affected by hydrothermal alteration. At Weld Range, primary amphiboles were preserved during lower greenschist facies regional metamorphism. Metamorphic chlorite appears to have inherited the Fe/Mg ratios of the parent rock, resulting in a compositional distribution with depth that matches primary amphibole. Several other ASTER geoscience products have been identified for detecting mafic igneous rocks, including MgOH-carbonate abundance and FeOH group abundance products, which identify rocks that comprise chlorite, epidote, amphibole, talc, or serpentine (Duuring et al., 2012).

In BIF, outer and inner hypogene alteration zones can be accurately mapped using quartz abundance and carbonate abundance or carbonate chemistry signatures (using a combination of TIR and SWIR data). A decrease in the quartz abundance signature is most robust and widely applicable because it can be used for fresh or weathered rocks, and it identifies hypogene and supergene iron ores. The carbonate chemistry product derived from SWIR data distinguishes Fe- and Mg-rich carbonates from calcium carbonates; the latter carbonates are less likely to be related

to hypogene iron ores. However, the carbonate abundance and chemistry signatures may have a more restricted use because carbonates are less likely to survive in supergene environments, or they may represent primary lithological facies distinctions (i.e. silica-facies vs carbonate-facies BIF) rather than a hypogene alteration feature.

Hypogene alteration zones in fresh mafic igneous rocks display a relative increase in the abundance of hypogene chlorite and a decrease in primary amphibole and plagioclase with proximity to BIF-hosted magnetite–martite ore zones. A ratio of these hyperspectral signatures would be an effective means to locate proximal alteration zones in fresh mafic rocks. However, weathering and primary compositional variations would add complexity that could reduce the accuracy of this index.

Contrary to expectations, mafic igneous rocks in this drillhole did not show measurable changes in alteration mineral chemistry associated with hypogene alteration zones. For example, there is no significant difference in chlorite chemistry with proximity to BIF-hosted, magnetite-rich ore zones. Nor did proximal alteration zones show the expected presence of talc. Furthermore, the increase in quartz abundance within 15 m of contacts with BIF is surprising considering that whole-rock geochemical data for these zones indicate that SiO_2 content commonly does not change, or is depleted. The absence of changes in the composition of chlorite in the WRRD0583 drillhole is surprising but might be specific to this drillhole located in the W9 prospect at the Beebyn deposit.

A comparison of ASTER geoscience products ('ferrous iron content in MgOH minerals', 'ferrous iron to silica index', and 'FeOH group abundance') for outcrop in the Beebyn deposit demonstrates that the broadest and most positive anomalies are located at the W11 prospect, about 3 km northeast of the W9 prospect (Duuring et al., 2012). The W9 prospect does not show clear anomalism in these geoscience products. A diamond drillhole located in the W11 prospect might be a better test for compositional differences in chlorite in mafic igneous country rocks.

Conclusions

Drillhole WRRD0583 located in the W9 prospect of the Beebyn deposit was scanned with the GSWA HyLogger-3 at the Perth Core Library. The hyperspectral data collected were compared with data collected from existing studies and data from conventional logging of the drillhole.

Hyperspectral data accurately distinguish rock types, mineral abundance, and mineral chemistry at a resolution of about 1 cm continuously down the drillhole. BIF and mafic igneous rocks are best distinguished using the opaque mineral abundance product. Variations in the detected Fe/Mg ratio for amphiboles (and hypogene chlorite) most likely indicate that there were multiple stages of intrusion of mafic igneous rocks.

High-grade hypogene magnetite–martite ore zones in BIF are accurately identified using the opaques abundance and quartz abundance products. A high ratio for opaques to quartz abundance corresponds to magnetite-rich, quartz-poor high-grade zones. High-grade, supergene goethite–hematite ore zones in BIF are best identified using a high goethite/hematite ratio and low quartz abundance signatures.

Contrary to expectations, no compositional differences were detected in hypogene chlorite associated with hypogene alteration zonation in mafic igneous country rocks located in the W9 prospect. This hypothesis might be better tested with the scanning of a drillhole located in the W11 prospect, where broad positive signatures were detected for iron-rich chlorite in mafic igneous rocks associated with BIF-hosted iron ore based on the interpretation of ASTER data.

Acknowledgements

This study was funded by the Geological Survey of Western Australia's Exploration Incentive Scheme (a Royalties for Regions initiative). We thank Sinosteel Midwest Corporation for providing access to drillhole WRRD0583.

References

Adams, JB and Filice, AL 1967, Spectral reflectance 0.4 to 2.0 microns of silicate rock powders: Journal of Geophysical Research, v. 72, no. 22, p. 5705–5715.

Angerer, T and Hagemann, SG 2010, The BIF-hosted high-grade iron ore deposits in the Archean Koolyanobbing greenstone belt, Western Australia: structural control on synorogenic- and weathering-related magnetite-, hematite-, and goethite-rich iron ore: Economic Geology, v. 105, p. 917–945.

Bishop, JL, Lane, MD, Dyar, MD and Brown, AJ 2008, Reflectance and emission spectroscopy study of four groups of phyllosilicates: smectites, kaolinite-serpentines, chlorites and micas: Clay Minerals, v. 43, no. 1, p. 35–54, doi:10.1180/claymin.2008.043.1.03.

Chiarelli, L 2015, Alteration mineral zonation associated with high-grade BIF-hosted iron ore: mineral mapping using hyperspectral drill core data: Geological Survey of Western Australia, Record 2015/3, 156p.

Clark, AM 1993, Hey's mineral index, mineral species, varieties and synonyms (3rd edition): Chapman and Hall, London, United Kingdom, 848p.

Clark, RN and Roush, TL 1984, Reflectance spectroscopy: Quantitative analysis techniques for remote sensing applications: Journal of Geophysical Research: Solid Earth, v. 89, no. B7, p. 6329–6340.

Cudahy, TJ, Jones, M, Thomas, M, Laukamp, C, Caccetta, M, Hewson, RD, Rodger, AR and Verrall, M 2008, Next generation mineral mapping: Queensland airborne HyMap and satellite ASTER surveys 2006–2008: CSIRO, Open File Report P2007/364, 120p.

Cudahy, TJ and Ramanaidou, ER 1997, Measurement of the hematite:goethite ratio using field visible and near-infrared reflectance spectrometry in channel iron deposits, Western Australia: Australian Journal of Earth Sciences, v. 44, no. 4, p. 411–420, doi:10.1080/08120099708728322.

Duke, E 1994, Near infrared spectra of muscovite, Tschermak substitution, and metamorphic reaction progress: Implications for remote sensing: Geology, v. 22, p. 621–624.

Duuring, P and Hagemann, SG 2013, Leaching of silica bands and concentration of magnetite in Archean BIF by hypogene fluids: Beebyn Fe ore deposit, Yilgarn Craton, Western Australia: Mineralium Deposita, v. 48, p. 341–370.

Duuring, P, Hagemann, SG, Novikova, J, Cudahy, T and Laukamp, C 2012, Targeting iron ore in banded iron formations using ASTER data: Weld Range greenstone belt, Yilgarn Craton, Western Australia: Economic Geology, v. 107, no. 4, p. 585–597.

Gallagher, R 2013, Hashimoto high-grade martite–goethite (M-G), martite – microplatey hematite (M-(mplH)) iron ore deposit — towards understanding ore genesis and associated alteration zoning: The University of Western Australia, MSc thesis (unpublished), 58p.

Geological Survey of Western Australia 2016, 1:500 000 State interpreted bedrock geology of Western Australia, 2016: Geological Survey of Western Australia, digital data layer, <www.dmp.wa.gov.au/geoview>.

Haest, M, Cudahy, T, Laukamp, C and Gregory, S 2012a, Quantitative mineralogy from infrared spectroscopic data. (I) Validation of mineral abundance and composition scripts at the Rocklea channel iron deposit in Western Australia: Economic Geology, v. 107, no. 2, p. 209–228.

Haest, M, Cudahy, T, Laukamp, C, and Gregrory, S 2012b, Quantitative mineralogy from visible to shortwave infrared spectroscopic data. (II) Three-dimensional mineralogical characterization of the Rocklea Dome channel iron deposit, Western Australia: Economic Geology, v. 107, no. 2, p. 229–249.

Haest, M, Mittrup, D and Hacket, A 2014, How hyperspectral sensing is improving productivity in BHP Billiton iron ore exploration, *in* Abstract No 110 of the 22nd Australian Geological Convention: Geological Society of Australia; 2014 Australian Earth Sciences Convention (AESC), Sustainable Australia, Newcastle, New South Wales, Australia, 7 July 2014, p. 90.

Hunt, G 1977, Spectral signatures of particular minerals in the visible and near infrared: Geophysics, v. 42, no. 3, p. 501–513, doi:10.1190/1.1440721.

Laukamp, C 2011, Short Wave Infrared Functional Groups of Rock-forming Minerals: CSIRO, Report EP115222, 13p.

Laukamp, C, Caccetta, M, Chia, J, Cudahy, T, Gessner, K, Haest, M, Liu, YC, Ong, C and Rodger, A 2010, The uses, abuses and opportunities for hyperspectral technologies and derived geoscience information: AIG Bulletin; Geo-Computing 2010 Conference, Brisbane, September 2010, no. 51, p. 73–76.

Laukamp, C, Termin, KA, Pejcic, B, Haest, M and Cudahy, T 2012, Vibrational spectroscopy of calcic amphiboles — applications for exploration and mining: European Journal of Mineralogy, v. 24, no. 5, p. 863–878.

Maskell, A, Duuring, P and Hagemann, SG 2014, Hydrothermal alteration events controlling magnetite-rich iron ore at the Matthew Ridge prospect, Jack Hills greenstone belt, Yilgarn Craton: Australian Journal of Earth Sciences, v. 61, no. 1, p. 187–212, doi:10.1080/08120099.2013.806359.

Sherman, DM, Burns, RG and Burns, VM 1982, Spectral characteristics of the iron oxides with application to the Martian bright region mineralogy: Journal of Geophysical Research: Solid Earth, v. 87, no. B12, p. 10169–10180.

Singer, RB and Roush, TL 1985, Effects of temperature on remotely sensed mineral absorption features: Journal of Geophysical Research: Solid Earth, v. 90, no. B14, p. 12434–12444.

Sonntag, I, Laukamp, C and Hagemann, SG 2012, Low potassium hydrothermal alteration in low sulfidation epithermal systems as detected by IRS and XRD: An example from the Co-O mine, Eastern Mindanao, Philippines: Ore Geology Reviews, v. 45, p. 47–60.

Appendix

Description of spectral scripts for geoscience products

Product name	Minerals detected	Base algorithm	Filters/Masks	Lower stretch limit	Upper stretch limit (based on UGD1683)	Related publication	Comments on general accuracy
Opaques abundance	Sulfides, carbon black (e.g. ash, magnetite, or Mn oxides)	(R456)/(R1650) OPAQUES_450D1650	albedo @ 1650 nm <30%	0.25: low content	Not specified yet – depending on results from other drillcores		Moderate: errors introduced by a lack of Fe^{3+} absorption in the visible, e.g. iron oxide poor clays that, in theory, would be masked by the <30% albedo but may be in partial 'shadow'
Ferric oxide abundance (Ferric_oxide_abundance.txt)	Hematite, goethite, jarosite	Continuum removed depth of the 900 nm absorption calculated using a fitted 2nd order polynomial between 776 and 1050 nm. 900D	R450 > R1650	0.04: low content	Not specified – depending on whole dataset	Further developed on the basis of Haest et al. (2012a,b), which used a 4th order polynomial or 4 band ratio approach	Low at Stavely: compromised by other tranistion metal-bearing minerals (e.g. pyroxene). High in regolith and iron ore deposits (Rocklea case study: RMSE = 9.7%)
hem/goe (Hematite-goethite.txt)	Hematite/goethite ratio	Continuum removed wavelength of the 900 nm absorption minimum calculated using a fitted 12th order polynomial between 776 and 1150nm. 900W	R450 > R1650 + 900D >0.025	~900 nm: more hematitic	~940 nm: more goethitic	Haest et al. (2012a,b)	Moderate: wavelength accuracy of the iron-oxide crystal field absorption is adversely affected by mixing with green and dry vegetation as well as ferrous-bearing carbonate and silicate minerals
Kaolin abundance (Kaolin_abundance_2011v2.txt)	Kaolin group minerals: kaolinite halloysite, dickite and nacrite	2200D (Normalized depth of a fitted 4th order polynomial between 2120 and 2245 nm)	2160D [(R2138+R2190)/(R2156+R2179)] >1.005	0.04: low content	Not specified – depending on whole dataset	Sonntag et al. (2012)	High in regolith, low in low-metamorphic grade rocks: compromised by pyrophyllite and prehnite
Kaolin composition (Kaolin_comp_2011v2.txt)	Composition and crystallinity of kaolin group minerals ranging from well-ordered kaolinite to halloysite to dickite (and nacrite)	[(R2138+R2173)/R2156]/[(R2156+R2190)/R2173]	2200D>0.005	not specified yet – depending on results from other drillcores	Not specified – depending on whole dataset	Sonntag et al. (2012)	Moderate, but compromised by pyrophyllite and prehnite
White mica abundance (wmAlsmai.txt)	Abundance of white micas (e.g. illite, muscovite, paragonite, brammalite, phengite, lepidolite, margarite) and smectites (montmorillonite, beidellite)	Relative absorption depth of the 2200 nm absorption for which the continuum is removed between 2120 and 2245, determined using a 3 band polynomial fit around the band with the lowest reflectance. 2200D3pfit	(R2326+R2376)/(R2343 + R2359) 2350DE >0.00035) + ((R2138+R2190)/(R2156 + R2179) 2160D2190 <1.063	0.04: low content	Not specified – depending on whole dataset	Further developed on the basis of Sonntag et al. (2012), which used a 4th order polynomial or 4 band ratio approach	Moderate: inherent errors related to the process of masking rather than umixing. That is, the threshold levels on mask parameters could exclude or include other materials especially for 'lower' levels. In sedimentary rocks at Stavely, problems with overlapping kaolinite
White mica composition (wmAlsmci.txt)	Tschermak substitution of white micas, ranging from paragonite, brammalite, to illite, muscovite to phengite, and smectites, ranging from beidellite to montmorillonite	Minimum wavelength of the 2200 nm absorption for which the continuum is removed between 2120 and 2245, determined using a 3 band polynomial fit around the band with the lowest reflectance. 2200W3pfit	(R2326+R2376)/(R2343 + R2359) 2350DE >0.00035) + ((R2138+R2190)/(R2156 + R2179) 2160D2190 <1.063	2185 nm: Al-rich mica (muscovite, illite, paragonite, brammalite, lepidolite)	2220 nm: Al-poor mica (~phengite)	Further developed on the basis of Sonntag et al. (2012), which used a 4th order polynomial or 4 band ratio approach	High: internationally established parameter for tracking Tschermak exchange in white micas and Al-smectites (e.g. Duke, 1994)
Chlorite–epidote abundance (chlepai3pfit.txt)	Chlorite, epidote, biotite	Relative absorption depth of the 2250 nm absorption for which the continuum is removed between 2230 and 2270, determined using a 3 band polynomial fit around the band with the lowest reflectance. 2250D3pfit	2250D3pfit >0.01, 2230 nm < 2250W < 2270 nm	0.04: low content	Not specified – depending on whole dataset	Further developed on the basis of Sonntag et al. (2012), which used a 4th order polynomial or 4 band ratio approach	Moderate: can be influenced by abundant jarosite, tourmaline, phlogopite. Probably some correlation with ferrous iron abundance
Chlorite–epidote composition (chlepci3pfit.txt)	Chlorite, epidote, biotite	Relative absorption depth of the 2250 nm absorption for which the continuum is removed between 2230 and 2270, determined using a 3 band polynomial fit around the band with the lowest reflectance. 2250D3pfit	2250D3pfit >0.01, 2230 nm < 2250W < 2270 nm	2248 nm: Mg-rich (Bishop et al., 2008)	2261 nm: Fe-rich (Bishop et al., 2008)	Further developed on the basis of Sonntag et al. (2012), which used a 4th order polynomial or 4 band ratio approach	Moderate: can be influenced by abundant jarosite, tourmaline, phlogopite. Probably some correlation with ferrous iron abundance
Carbonate abundance index TIR (6500P_3pfit.txt)	Calcite, dolomite, magnesite, siderite, ankerite	6500P Relative height of the reflectance peak between 6300 and 6700 nm, determined using a 3 band polynomial fit around the band with the highest reflectance		0.1	Not specified – depending on whole dataset	Inherited, unpublished	High, but lower threshold dependent on dataset
Carbonate composition index TIR1 (14000DW_3pfit.txt)	Calcite, dolomite, magnesite, siderite, ankerite	14000DW Minimum wavelength of the reflectance low between 13000 and 14000 nm, determined using a 3 band polynomial fit around the band with the lowest reflectance		13000 nm: Mg/Fe-rich	14000 nm: Ca-rich	Inherited, unpublished	High, but lower threshold dependent on dataset
Carbonate abundance (Carbonate_abundance_SWIR.txt)	Carbonates vs MgOH-bearing silicates, based on left-asymmetry of CO_3 feature @ 2340	Relative absorption depth of the 2340 nm absorption for which the continuum is removed between 2270 and 2370, determined using a 3 band polynomial fit around the band with the lowest reflectance. 2340D	2340D >0.04, 2295 nm < 2340W < 2360 nm, 2250D < 0.025, 2380D < 0.1117*2340D + 0.0002, Asymmetry of the 2340 absorption using a fitted 4th order polynomial between 2120 and 2370: 2340_left_asym > 1.13	0.05: low content	Not specified – depending on whole dataset	Further developed on the basis of Sonntag et al. (2012), which used a 4th order polynomial or 4 band ratio approach	Low: heavily impacted by grain size effects. False positives in case of mineral mixtures of, for example, white mica and chlorite
Carbonate composition SWIR (Carbonate_composition_SWIR.txt)	Separating calcite, dolomite, and siderite	Minimum wavelength of the 2340 nm absorption for which the continuum is removed between 2270 and 2370, determined using a 3 band polynomial fit around the band with the lowest reflectance. 2340W	2340D >0.04, 2295 nm < 2340W < 2360 nm, 2250D < 0.025, 2380D < 0.1117*2340D+0.0002, Asymmetry of the 2340 absorption using a fitted 4th order polynomial between 2120 and 2370: 2340_left_asym > 1.13	2303 nm: magnesite; 2326 nm: dolomite; recommendation for Stavely dataset: 2320 nm	2343 nm: calcite; recommendation for Stavely dataset: 2320 nm	Further developed on the basis of Sonntag et al. (2012), which used a 4th order polynomial or 4 band ratio approach	Moderate: works well for those carbonates, which are not masked out by the carbonate abundance index SWIR, The latter should be replaced by carbonate abundance index TIR
Amphibole–talc abundance (Amph_Talc_abundance.txt)	Abundance of amphibole and talc	2380D [(R2365+R2415)/(R2381+R2390)]	Composite mask* + MgOH abundance > 1.01 (+ 2160D2190 < 1.005)	1.005: low content	Not specified – depending on whole dataset	Laukamp et al. (2012)	Moderate: can be compromised by abundant phlogopite; noise
2080D3 (2080D3pfit.txt)	Depth of the 2080 feature, evident in talc. Useful for separating talc from amphiboles, the latter in general not showing this absorption feature	Depth of the 2080 nm absorption feature, for which the continuum is removed between 2060 and 2100, determined using a second order polynomial fitted through the 3 bands with the lowest reflectance. 2080D				Laukamp et al. (2012)	
2390W (2390W3pfit.txt)	Estimate of the Mg/Fe ratio (Mg#) in, for example, amphiboles and talc	Wavelength of absorption minimum calculated using a fitted fourth order polynomial between 2365 and 2430 nm, focused between 2380 and 2410 nm. 2390W		2382 nm: Mg-rich (Laukamp et al., 2012)	2406 nm: Fe-rich (Laukamp et al., 2012)	Laukamp et al. (2012)	
Quartz abundance	Quartz	8635D Relative depth of the 8626 nm Reststrahlen feature for which the continuum is removed between 8565 and 8705 nm, determined using a 3 band polynomial fit around the band with the lowest reflectance	no mask	0.1	Not specified – depending on whole dataset	Inherited, unpublished	High, but lower threshold dependent on dataset. Fractured drillcore can lead to extreme overestimation

References:

Bishop, JL, Lane, MD, Dyar, MD and Brown, AJ 2008, Reflectance and emission spectroscopy study of four groups of phyllosilicates: smectites, kaolinite-serpentines, chlorites and micas: Clay Minerals, v. 43, p. 35–54

Duke, E 1994, Near infrared spectra of muscovite, Tschermak substitution, and metamorphic reaction progress: Implications for remote sensing: Geology, v. 22, p. 621–624.

Haest, M, Cudahy, T, Laukamp, C and Gregrory, S 2012a, Quantitative mineralogy from visible to shortwave infrared spectroscopic data. (I) Validation of mineral abundance and composition products of the Rocklea Dome channel iron deposit in Western Australia: Economic Geology, v. 107, p. 209–228.

Haest, M, Cudahy, T, Laukamp, C and Gregrory, S 2012b, Quantitative mineralogy from visible to shortwave infrared spectroscopic data. (II) Three-dimensional mineralogical characterisation of the Rocklea Dome channel iron deposit, Western Australia: Economic Geology, v. 107, p. 229–249.

Laukamp, C, Termin, KA, Pejcic, B, Haest, M and Cudahy, T 2012, Vibrational spectroscopy of calcic amphiboles – applications for exploration and mining: European Journal of Mineralogy, v. 24, p. 863–878.

Sonntag, I, Laukamp, C and Hagemann, S 2012, Low potassium hydrothermal alteration in low sulfidation epithermal systems as detected by IRS and XRD: an example from the Co-O Mine, Eastern Mindanao, Philippines: Ore Geology Reviews, v. 45, p. 47–60.

RECORD 2016/16

MAPPING IRON ORE ALTERATION PATTERNS IN BANDED IRON-FORMATION USING HYPERSPECTRAL DATA: BEEBYN DEPOSIT, YILGARN CRATON, WESTERN AUSTRALIA

Duuring and Laukamp

This Record is published in digital format (PDF) and is available as a free download from the DMP website at <www.dmp.wa.gov.au/GSWApublications>.

Further details of geological products produced by the Geological Survey of Western Australia can be obtained by contacting:

Information Centre
Department of Mines and Petroleum
100 Plain Street
EAST PERTH WESTERN AUSTRALIA 6004
Phone: +61 8 9222 3459 Fax: +61 8 9222 3444
www.dmp.wa.gov.au/GSWApublications